Nuclear Instruments and Methods 199 (1982) 531-548
North-Holland Publishing Company

MORE REALISTIC MONTE CARLO CALCULATIONS OF PHOTON DETECTOR RESPONSE FUNCTIONS

D.W.O. ROGERS

Division of Physics, National Research Council of Canada, Ottawa K1A OR6, Canada

Received 5 November 1981

The Monte Carlo electron-photon simulation package EGS3 has been used to calculate response functions for a wide variety of nuclear detectors. The detectors must be cylindrical and can be encased in a jacket or shielded by a plate of arbitrary material. The detector can have inert volumes. The code, via EGS, includes all physical processes necessary for accurate calculations for incident photons above 300 keV. An error in EGS concerning terminal processing of positrons has been found and corrected. The code runs 3 to 5 times faster than CYLTRAN. The paper presents benchmark comparisons between EGS and a wide variety of previous NaI and Ge(Li) response function calculations, in particular those of ETRAN where small but systematic differences were observed above 10 MeV incident energy. The effects of detector cladding and shielding have been studied. The program quantitatively explains the effects of a 1.18 g/cm^2 Be beta absorber and qualitatively explains the 511 keV peak present for incident high energy photons. To first order it was found that only for the photopeak efficiencies can the effect of material in front of a detector be treated as a simple absorption. The reduction in the efficiency for counts within 1.5 MeV of the incident energy is considrably less than expected using only the cross section and the reduction for escape peaks is significantly more due to reflections of 511 keV photons back into the detector. Calculations of absolute Ge(Li) detector efficiency were found to be difficult due to sensitivity to inert layer parameters but relative efficiency curves were much less sensitive. Calculations are included of response functions for bismuth germanate and large NaI detectors and angular scans of Ge(Li) detectors for solid angle correction factors. Difficulties calculating electron response functions are discussed.

1. Introduction

The response functions of NaI, Ge and Si detectors to photons and electrons have been the subject of many Monte Carlo studies [1-13]. Many of these studies had serious restrictions on their applicability. Virtually none of these studies has included the effects of the jacket surrounding the active detector element and yet, in a mono-energetic beam of 6 MeV photons, the tallest peak in the spectrum recorded with a 5″ × 4″ NaI detector shielded by a 3 mm lead filter is the 511 keV peak caused by pair production in the jacket; further, the lead reduces the calculated photofraction by 20%. Many studies have also used simplified radiation transport models which have left out various physical processes. The most frequent simplification is to ignore transport of charged particles and assume they deposit all their energy where they are created. For low energies this is a good approximation but even at 2.75 MeV it causes a 20% error in the calculated photofraction for a 3″ × 3″ NaI detector and at 6 MeV the results are substantially wrong if particle transport is ignored.

This paper reports the development of a versatile and easily extended user code called JACKET which uses the EGS Monte Carlo simulation package. It has the following characteristics:

1) It can calculate the response of NaI, Ge, Si, $Bi_4Ge_3O_{12}$ or nuclear detectors of any material.

2) The detector must be cylindrical in shape but inert volumes are allowed in order to simulate open or closed ended coaxial Ge(Li) detectors with an inert dead layer on the surface.

3) The detector may be clad in a jacket of arbitrary material, with varying thicknesses on the front, back and sides. Calculations are reported here for jackets of Al, Pb, Al_2O_3, Be, lucite and polystyrene. With minor modifications the jacket could be treated as an anti-coincidence shield.

4) The simulation takes into account all physical processes required to calculate the detector's response to photons above 300 keV (up to 100 GeV).

5) Various source routines can be specified, such as parallel beams of arbitrary radius and angle with respect to the front face or an isotropic point source on the axis.

6) The code is written using the EGS3 code system developed at SLAC by Ford and Nelson [14].

7) For the same problem, JACKET runs 3 to 5 times faster than Sandia Lab's CYLTRAN [15] which is an extended version of the NBS code ETRAN [2,3].

Section 2 of this paper outlines the characteristics of the EGS system and the minor modifications made at

0167-5087/82/0000-0000/$02.75

NRCC. Section 3 discusses the particular characteristics of the user's code JACKET. The following sections compare the results of JACKET to previous calculations for NaI, Ge and Si detectors and to results obtained using CYLTRAN (ETRAN). Section 5 includes a detailed discussion of the effects of the detector's cladding on NaI response functions. Section 7 discusses several applications of the code to other situations [70 MeV e^+ on NaI, Ge(Li) attenuation coefficients, bismuth germanate detectors, electron detectors].

The following symbols and nomenclature are used throughout the paper:

ε°	– photofraction = fraction of counts in spectrum which are in the full energy peak;
ε', ε''	– the fraction of counts in the spectrum which are in the single and double escape peaks respectively;
ε_K	– the fraction of the counts in the spectrum which are within 1.5 MeV of the incident photon's energy
ε_{tot}	– for parallel beams of incident particles – the number of counts in the spectrum per particle or photon which would hit the detector element if it were bare;
	– for isotropic point sources – the number of counts in the spectrum per particle or photon leaving the source unless primed in which case it has the same meaning as the parallel beam case;
0.123(t)	– the number in the bracket is the uncertainty in the last digit calculated as an estimate of the one standard deviation limit
[700,100]	– indicates the electron and photon cut-off energies respectively, used in the calculation. The electron energy refers to the total energy (= kinetic energy +511 keV).

2. The EGS code system

The EGS code system is a well structured and thoroughly documented system of programs which allow the user to simulate electromagnetic cascade showers in any material. Essentially the user writes: (1) a user code (or main program) which handles input, output and initialization of various parameters; (2) a subroutine to specify the geometry of the particular problem; and (3) a scoring routine which keeps track of the quantities of interest (in this case the energy deposited in the active detector volume). The preparation of the data files required for a particular set of materials is handled by a separate program called PEGS. The physical processes considered and the models used to simulate them are briefly reviewed below (see ref. 14 for a detailed description).

2.1. Compton scattering

The Compton cross sections for photon scattering from electrons are obtained from the Klein–Nishina formula which applies to free electrons. Binding effects, which can make substantial adjustments to the Compton cross section at low energies, are ignored since Compton scattering makes a small contribution relative to the photoelectric effect in these energy regions. Coherent Rayleigh scattering (which only deflects the photons) is not considered.

2.2. Photoelectric effect

The cross sections for the photoelectric effect are taken directly from Storm and Israel's tables [16]. After the photoelectric event, the version of EGS being used creates and tracks a photoelectron going in the same direction that the photon had been going, with an energy equal to the photon energy less a weighted average energy of the K-edges in the material. The remaining energy is considered to be deposited at the point of interaction rather than appearing as K X-rays, Auger electrons etc. It is this simplified treatment which sets the lower limit on the photon energy for which response functions can be calculated.

2.3. Pair production

Below 50 MeV, empirically corrected Born approximation cross sections are used for pair production and above 50 MeV extreme relativistic Coulomb corrected cross sections are used. The screening corrections use Thomas–Fermi form factors. The data from Storm and Israel for total pair production cross sections are used for the empirical correction factors below 50 MeV. The code does not account for triplet production in the field of the atomic electrons except via the total cross section (i.e. the triplet cross section is included but treated as if a pair were produced). This shortcoming has no effect in the current calculations since triplet production would only be significant in a pure, low Z material because $\sigma_{triplet}/\sigma_{pair}$ which is ~ 0.5 for $Z=1$, varies as $1/Z$ and σ_{pair} varies as Z^2: hence even a small amount of heavy Z material dominates the pair production process.

For pair production with $E_\gamma \leq 2.1$ MeV the approximation is made that one member of the pair is at rest and the other carries all the energy away.

2.4. Bremsstrahlung production

Bremsstrahlung production by a slowing electron or positron is closely related to the pair production process. Its cross sections are similarly obtained from empirically corrected Born approximations for $E \leq 50$ MeV and from the extreme, relativistic Coulomb corrected cross sections above 50 MeV. The same Thomas–Fermi form factors are used for the screening corrections. The empirical corrections are obtained from the review of Koch and Motz (fig. 23, ref. 17). The same comments that applied to triplet production above apply to bremsstrahlung production in the field of an atomic electron. EGS also ignores the Elwert correction factor to the cross section for bremsstrahlung production by electrons with energies below 2 MeV (ref. 17).

When an electron radiates a photon, the electron's direction is considered unchanged since the deflection is small compared to multiple scattering. The photon is given off at an angle of $\theta = 0.511/E_e$.

2.5. Positron annihilation

EGS allow for in flight positron annihilation using the cross section of Heitler [18]. A correction to the EGS system was made at NRCC to ensure that thermalized positrons always create two photons on annihilation since positron histories terminated by the user energy cut-off in the original version did not create photons unless their energies were also lower than the PEGS energy cut-off.

2.6. Electron/positron scattering

As an electron or positron slows down in a material it undergoes thousands of elastic scatterings which change its angle but have little effect on its energy. To make this problem tractable using Monte Carlo techniques, a condensed history technique is used in which the electron is transported through a small distance and then, if no other interaction occurs, the angle of deflection due to the multiple scattering is determined using the theory of Moliere as formulated by Bethe [19]. This formulation is considered accurate down to electron kinetic energy of about 1 MeV. Below this energy the theory of Goudsmit and Saunderson [20] should be used since it more accurately accounts for occasional large angle scatterings. However, in photon detector response calculations, this should not make a significant difference since we are interested in energy depostion rather than the angular distribution of electrons.

The elastic scattering of electrons and positrons is taken into account using the cross sections of Møller and Bhabha as formulated by Messel and Crawford [21]. In practice and electron cut-off energy must be chosen such that collisions creating electrons with energies less than this energy are treated as part of the continuous energy loss mechanism and the secondary electrons are not followed. The running time of the code is strongly dependent on the value choosen for this cut-off (e.g. a 6 MeV beam incident on a 5″ × 4″ crystal takes 20 times as long to simulate with an electron cut-off of 20 keV as with a cut-off of 1 MeV, see appendix for a discussion of timing effects).

2.7. Continuous electron/positron energy loss

When traversing a medium, electrons and positrons lose energy by radiating bremsstrahlung and by elastic collisions. If the resulting secondary photons or electrons have energies less than specified energy cut-offs, energy loss is considered local in nature and treated as a continuous process. The total continuous energy loss per unit length is the sum of a term which is derived by integrating the bremsstrahlung cross section (described above) for photons up to the photon cut-off energy, and a term which gives the ionization stopping power restricted to electrons below the electron cut-off energy. EGS uses the Bethe–Bloch formula for the restricted stopping power as given by Berger and Seltzer [22]. The density effect is handled using Sternheimer's explicit formulae where available or using the asymptotic density effect correction as suggested by Armstrong and Alsmiller [23]. The values of the average adjusted ionization energy are those used by Berger and Seltzer [22] and Sternheimer [24].

2.8. NRCC modifications

Four minor modifications or extensions to the EGS system have been implemented at NRCC. The most significant for the present calculations was the correction to the terminal handling of positrons discussed in section 2.5. This problem caused serious errors if user energy cut-offs were different from the PEGS energy cut-offs. Secondly, in order to reduce the stack size, a minor modification was made to the way the electrons and photons resulting from a Compton scattering were placed on the stack. Thirdly, an extra variable was added to the stack which allowed information to be passed along about the parentage of any particle (e.g. bit 2 was set if any ancestor had interacted in the detector's jacket). Finally, a random number generator was used which ensured no correlations in triples of random numbers (as is common for the usual routines – see e.g. refs 25 and 26).

3. The code JACKET

JACKET consists of a main program and seven subroutines which use the EGS system to simulate energy deposition in an encapsulated nuclear detector.

JACKET and EGS are written in MORTRAN, an extended FORTRAN language developed at SLAC [27] which facilitates structuring the code. No variance reduction techniques have been used.

Statistical uncertainties are computed by doing the calculation in an arbitrary number of batches (10) and using the variation in the batch results to estimate the uncertainty in the final value which is the mean of the batch values. Another feature is that whenever a calculation is done for an encapsulated detector, the results are calculated for the bare detector in the same geometry by ignoring all energy deposited in the detector after a particle or its ancestor has interacted in the jacket. After properly normalizing the results it is possible to deduce the effect of the jacket by subtraction. Since the calculated bare and clad spectra are highly correlated (most events are the same), variance on the difference is much smaller than would be expected if the difference were taken between separate calculations for the bare and clad cases.

The code calculates the total efficiencies for both the bare and clad detector in each case. For the case of an isotropic source on the detector axis the natural definition of efficiency is counts per source particle. For parallel beams of particles, efficiency is defined as counts per particle which would hit the sensitive element's front face if there were no cladding. With these definitions, the total efficiency for the clad detector is usually higher than for the bare detector because of inscattering from the radial walls (assuming the incident beam hits them) which more than compensates for those particles stopped by the cladding on the front face.

For comparison sake, all source to detector distances refer to the distance to the front face of the sensitive material (not the jacket).

In each case, JACKET calculates ε, ε', ε'' and ε^{511}. These are the fraction of the counts in the response spectrum which are in the full energy (E_0), single escape ($E-511$ keV), double escape (E_0-1022 keV) and 511 keV peaks respectively (ε°, ε' and ε'' correspond to Berger and Seltzer's P_0, P_1 and P_2 [2]). The values are calculated by setting peak bins of arbitrary width (defaulting to 10 keV) around the energies of interest and background bins of half the width immediately above and below the peak bins. Calculated values were found to be insensitive to the chosen bin width. Note that the peak at 511 keV is the result of pair production events in the jacket and does not appear in any calculated bare case.

Another feature of the code, useful for debugging, is an option to list all interactions and their resulting particles. For example, a single 25 MeV photon leads to as many as 50 particles (electrons, positrons or photons) being tracked in a large NaI detector.

In terms of running the code, the major critical parameters are the source geometry, the number of histories to follow and the energy cut-offs to use (the energies below which electrons or photons are deemed to loose all their energy locally). Lower limits on the cut-offs are set by values in the data files prepared by PEGS, the data preprocessor part of the EGS system. The user can override these and as discussed in the appendix, considerable time savings are available with little loss of accuracy.

4. Program verification

To verify a program of this complexity and versatility is difficult. The EGS system has been extensively used previously but it is being used near its low energy limit for these calculations and in fact several minor errors have been uncovered. In the following sections fairly extensive comparisons to previous calculations for various types of detectors will be given in order to benchmark the EGS system and to verify the users code JACKET.

5. Response functions for NaI detectors

5.1. Comparison with previous NaI calculations

5.1.1. Bare NaI crystals

Table 1 compares the photofractions obtained via the EGS code (with and without electron transport) with those from five previous studies. The studies of Belluscio et al. [1] and Giannini et al. [7] used simplified models of electron transport and bremsstrahlung production. Within their limited statistical accuracy their results are in agreement with ours. By digitizing Giannini et al.'s fig. 3 comparison can be extended to 15 MeV. Good agreement is obtained for a point source 10 cm from a 3″ × 3″ detector and similar comparisons for a broad parallel beam show reasonable agreement with a slight tendency for ours to be smaller. However agreement is not obtained with Giannini et al's value of ε' for a 12 MeV broad beam as quoted by Berger and Seltzer [2] (see discussion below).

The photofractions of Zerby and Moran [13] are lower than those calculated by EGS (they are 18–35% lower between 2.75 and 5 MeV). However, using a version of their code here at NRCC, it was found that the values of ε_K calculated by MORN tend to be larger than those calculated by EGS.

The values of Steyn et al. [12] are in good agreement if no electron transport or brem production are included in the EGS calculation, although it is clear these have a significant effect, even at 2.7 MeV.

In table 1, the EGS results for the photofraction of a 3″ × 3″ detector do not agree very well with those of Grosswendt and Waibel [8] whose calculated results are 17–20% lower (but with a statistical uncertainty of about 10%). However the EGS results are in much better agreement with Waibel and Grosswendt's [9] experimental values than their calculations (see section 5.3). There is good agreement with their calculated

Table 1
Calculated photofractions (ε°) for isotropic point sources 10 cm from a bare 3″×3″ NaI detector.

E_{γ} (MeV)	EGS No electron transport	EGS [700,100] [e]	Steyn et al. [12]	Zerby and Moran [13]	Belluscio et al. [1]	Giannini et al. [7] [c]	Grosswendt and Waibel [8]
0.320	–	0.829(7)	0.845	0.85	0.85(4)	0.835	–
0.662	0.575(3)	0.576(9)	0.571	0.58	0.57(4)	0.551	0.52
1.28	0.395(3)	0.381(5)	0.402	0.36	–	0.380	0.35
2.75	0.266(5)	0.232(7)	0.268	0.19	0.24(2)	0.229	0.19
4.45 [a]	0.274(3)	0.222(4)	0.280	–	–	–	–
6.00	0.174(5)	0.108(5)	–	$0.094^{+.007}_{-.013}$	0.11(2)	0.100 [d]	0.086
8.00	0.159(4)	0.074(3)	–	–	0.080(2)	0.076	0.063
10.00	0.147(6)	0.053(1)	–	–	0.061(2)	0.055	0.047
12.00	–	0.039(1)	–	–	–	0.036 [b]	0.031
15.0	–	0.020(1)	–	–	–	0.020 [b]	0.0185

[a] 4″×4″.
[b] Interpolated.
[c] Taken from Belluscio et al.
[d] 6.1 MeV.
[e] Energy cut-offs used in the EGS calculation.

values for ε_K, the intrinsic efficiency for counts greater than $E_{\gamma} - 1.5$ MeV.

Grosswendt and Waibel have also calculated response functions for a point source at 55 cm collimated to illuminate the back face of a 33 × 27 cm² NaI detector. Table 2 shows there is up to a 10% difference for the absolute photopeak efficincies which is satisfactory considering their statistical accuracy of about 10%. There is excellent agreement for $\varepsilon_K \varepsilon'_{tot}$ with deviations of less than 2% over the entire energy range.

ETRAN is the most complete code previously used to calculate NaI response functions. It was developed by Berger and Seltzer at the NBS [2,3]. Table 3 demonstrates the excellent agreement obtained between EGS and ETRAN for the calculated photofraction at 662 keV. Fig. 1 shows the reasonable agreement obtained at another extreme, a broad parallel beam of 50 MeV photons incident on a 3″ × 3″ detector. Table 4 and fig. 2 compare the calculated responses of a 3″ × 3″ NaI detector to broad parallel beams of photons with energies up to 20 MeV. They demonstrate that at energies above 8 MeV there are relatively small but systematic differences between EGS and ETRAN, especially for ε' and ε''. An effort was made to resolve these differences using CYLTRAN [15], the Sandia Lab's extension of ETRAN which has been installed at NRCC. Despite

Table 2
Comparison of calculated intrinsic photopeak efficiencies ($\varepsilon^{\circ}\varepsilon'_{tot}$) and $\varepsilon_K \varepsilon'_{tot}$ the intrinsic efficiency for counts within 1.5 MeV of E_{γ} for a source at 55 cm collimated to illuminate the back face of a 33×27 cm² NaI detector.

E_{γ} (MeV)	$\varepsilon^{\circ}\varepsilon'_{tot}$ Grosswendt and Waibel [8]	$\varepsilon^{\circ}\varepsilon'_{tot}$ EGS+ [700,100]	$\varepsilon_K\varepsilon'_{tot}$ Grosswendt and Waibel [8]	$\varepsilon_K\varepsilon'_{tot}$ EGS [a] [700,100]
1	0.83	0.90	–	–
5	0.62	0.68	0.92	0.90
10	0.48	0.53	0.89	0.88
20	0.35	0.35	0.79	0.78
30	0.23	0.23	0.74	0.73
40	0.19	0.17	0.61	0.61

[a] Statistical uncertainty ≤1 in last digit in all cases.

Table 3
Comparison of photofraction (ε°) calculated with ETRAN [2] and EGS for pencil and broad beams of 662 keV photons incident on various bare NaI detectors.

Detector size	ε°			
	Pencil beam		Broad beam	
	ETRAN	EGS [a] [700,100]	ETRAN	EGS [a] [700,100]
1″×1″	0.384	0.380	–	0.323
2″×2″	0.574	0.578	0.478	0.478
3″×3″	0.703	0.701	0.569	0.586
4″×4″	0.790	0.795	0.664	0.665
5″×4″	0.818	0.824	0.698	0.696

[a] Statistical uncertainties ≤1% in all cases.

some problems running CYLTRAN (it is run on a 32-bit DEC VAX whereas it was developed on a 60-bit CDC machine), it appears to confirm the results obtained by Berger and Seltzer using ETRAN. However, when the CYLTRAN results are compared with those of EGS using wide energy bins (e.g. 500 keV), excellent agreement is obtained for a 12 MeV beam incident on a 3″ × 3″ detector. Alternatively, if the nunber of counts above $E_{\gamma} - 2$ MeV are considered for 12 or 20 MeV beams, there is agreement within the statistical uncertainty of about 3%, whereas there were 13% and 20% differences in the calculated ε' values. These differences in calculated values of ε' and ε'' are unexplained. However, from a practical point of view this difference is not important for NaI detectors since only efficiencies for detection above a certain threshold are important, and on this point the two codes appear to agree. The problem could be significant for Ge(Li) detectors at high photon energies.

5.1.2. Clad NaI crystals

Working within the no electron transport approximation, Steyn et al. [12] have calculated the effects of Al cladding on the response functions of NaI crystals for low energy photons. Tables 5 and 6 show comparisons between EGS and their results. Agreement is excellent if

Table 4
Comparison between EGS and ETRAN [2] of the calculated values of ε°, ε', ε'' and ε_{tot} for broad parallel beams of photons falling on a bare 3″×3″ NaI crystal.

E_{γ} (MeV)	ε°		ε'		ε''		ε_{tot}	
	ETRAN	EGS	ETRAN	EGS	ETRAN	EGS	ETRAN	EGS
0.3	0.875	0.879 (4)	–	–	–	–	0.988	0.989(5)
0.5	0.697	0.700 (3)					0.924	0.926(6)
0.8	0.534	0.519 (5)					0.843	0.832(6)
1.0	0.471	0.459 (6)					0.802	0.805(5)
1.5	0.370	0.358 (2)	0.0056	0.0058(6)	0.0025	0.0037(4)	0.728	0.725(2)
2.0	0.304	0.304 (6)	0.0234	0.0235(9)	0.0099	0.0095(7)	0.684	0.687(3)
3.0	0.225	0.218 (6)	0.0643	0.060 (4)	0.0257	0.029 (3)	0.641	0.659(6)
4.0	0.178	0.168 (5)	0.0979	0.091 (4)	0.0366	0.035 (3)	0.624	0.626(7)
5.0	0.143	0.138 (4)	0.114	0.101 (5)	0.0425	0.045 (2)	0.620	0.613(4)
6.0	0.117	0.114 (3)	0.119	0.113 (3)	0.0446	0.043 (3)	0.621	0.616(6)
8.0	0.0793	0.070 (5)	0.112	0.105 (3)	0.0419	0.035 (2)	0.629	0.626(6)
10.0	0.0567	0.056 (2)	0.0951	0.085 (5)	0.0327	0.030 (2)	0.643	0.642(4)
12.0	0.0425	0.040 (1)	0.0720	0.064 (1)	0.0248	0.022 (1)	0.656	0.658(2)
15.0	0.0259	0.021 (1)	0.0444	0.040 (1)	0.0161	0.0135(7)	0.675	0.674(3)
20.0	0.0092	0.0090(5)	0.0198	0.0165(8)	0.0074	0.0066(7)	0.702	0.705(3)

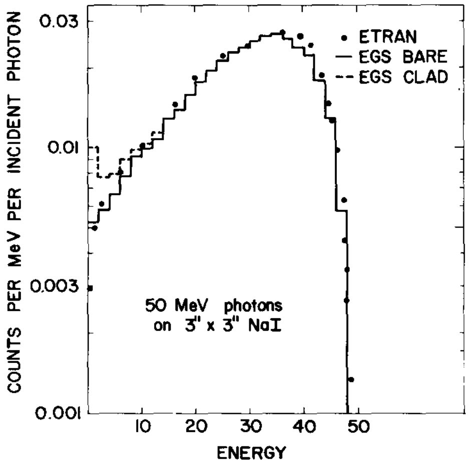

Fig. 1. Response function for a 3"×3" NaI detector in a broad parallel beam of 50 MeV photons. The EGS calculations were done using ECUT=2.0 MeV, and PCUT=0.1 MeV. The ETRAN [2] calculations are for a bare NaI. The EGS clad case was for a 3 mm jacket of Al_2O_3. The discrepancy at 40 MeV is statistically significant.

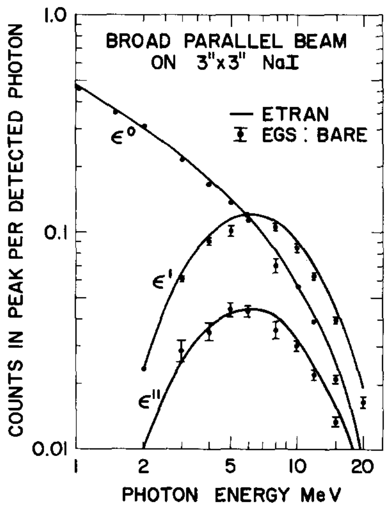

Fig. 2. Comparison of peak fractions ε°, ε' and ε'' calculated using EGS and ETRAN [2] for broad parallel beams of photons incident on a bare 3"×3" NaI. ETRAN results are shown by the smooth curves and EGS results by the points. The small discrepancies above 10 MeV are statistically significant but unexplained.

Table 5
Comparison with the results of Steyn et al. [12] for the effects of a front or side cladding of aluminium on the calculated photofraction ε°, in a 3"×3" detector irradiated by a 661 keV point source at 10 cm.

Side clad thickness (cm)	Photofraction			Front thickness (cm)	Photofraction		
	Steyn [a] et al.	EGS [2000,100] [b]	EGS [700,100]		Steyn [a] et al.	EGS [2000,100]	EGS [700,100]
0	0.57	0.57	0.564(7)	0	0.57	0.57	0.564(7)
0.32	0.56	0.56	0.546(8)	0.41	0.54	0.54	0.541(6)
1.27	0.52	0.51	0.513(9)	0.58	0.53	0.53	0.505(4)
2.54	0.48	0.47	0.456(6)	2.54	0.43	0.42	0.408(9)

[a] Scaled from fig. 8. of ref. 12.
[b] [ECUT,PCUT]=[2000,100] implies there is no electron transport, uncertainty ≤1 in last digit in all cases.

Table 6
Comparison with the results of Steyn et al. [12] for the photofraction ε° as a function of beam radius for 0.662 and 1.25 MeV parallel beams of photons incident on a 3"×3" NaI detector clad with 0.32 cm of Al on the front and side and 0.74 cm of Al at the back to simulate a photomultiplier tube. The cladding has roughly a 9% effect when the beam hits the side cladding and a 5% effect in other cases.

Beam diameter (cm)	ε_0 at 662 keV		ε_0 at 1.25 MeV		
	Steyn et al. [12]	EGS [700,100]	Steyn et al.	EGS [2000,100] [a]	EGS [700,100]
8.26	0.543	0.534(5)	0.385	0.376(3)	0.354(5)
7.62	0.552	0.572(5)	0.399	0.401(6)	0.381(5)
6.24	0.618	0.609(5)	0.438	0.421(8)	0.425(5)
0.17	0.668	0.680(5)	0.498	0.493(7)	0.470(7)

[a] Corresponds to no electron transport.

electron transport is excluded from the EGS calculation, although it is clear that it makes a difference even at these low energies.

A further check on the clad calculations has been done by comparing them to the results obtained using CYLTRAN. For a 5″ × 4″ NaI detector clad in a 1 cm jacket of Al, the calculated responses to a 6 MeV beam agreed within a statistical uncertainty of 3% for 500 keV bins.

5.2. Effects of jacket on NaI response functions

Most commercial NaI detectors are encased in containers between 3 and 10 mm thick. These typically consist of an aluminium can (~ 1–3 mm), some rubber or sponge (~ 1–3 mm) and reflector (1–3 mm of Al_2O_3 or MgO). In many experiments it is also common to have a lead filter around the detector to reduce low energy *X*-rays or to have a low *Z* filter as a beta absorber. There is also a photomultiplier at the rear of the crystal. All these materials contribute to the detector's response function. In this section the magnitude of these various effects is explored.

5.2.1. Effects of a beryllium beta absorber

There are few data published which can be quantitatively compared to the present calculations. Heath [28] has published curves showing the attentuation as a function of energy of the photopeak efficiency of a 3″ × 3″ NaI detector behind a 1.18 g/cm^2 Be beta absorber. Table 7 compares the experimental attenuation with the attenuation calculated by assuming that any interaction in the absorber removes the photon from the photopeak and with the attenuation calculated using EGS. The two calculations differ in that some photons scatter in the absorber but lose so little energy that they are experimentally counted in the photopeak. The EGS results are in good agreement with experiment. Fig. 6 presented in section 5.3 shows the effect of such a Be absorber on the measured response function.

Table 7
Attenuation of the absolute photopeak efficiency caused by a 1.18 g/cm^2 Be absorber in front of a 3″×3″ NaI detector.

E_γ (keV)	Experiment Heath [28]	Calculated	
		Total cross-section removal	EGS [a]
300	0.927	0.890	0.922
500	0.930	0.912	0.932
1000	0.943	0.937	0.947
2000	0.955	0.950	0.964

[a] Calculated by smearing the calculated response function using Heath's measured fwhm as a function of energy and then fitting a gaussian to the "photopeak" which includes some photons scattered in the Be. Things become difficult at 2 MeV where the Compton edge overlaps the low energy part of the peak.

5.2.2. Effects of Al/Al_2O_3 encapsulation

To study the effects of cladding, a series of calculations have been done for broad parallel beams of 0.661 and 6.13 MeV photons incident on a 3″ × 3″ NaI detector clad in varying thicknesses of Al.

The first conclusion is that the material behind the detector has only a minor effect on the response function. A 10 mm Al plate at the back changes ε° by about 0.6% at 0.661 and 6.13 MeV and has virtually no effect on the photopeak efficiency $\varepsilon^\circ\ \varepsilon_{tot}$.

Fig. 3 shows the effects on ε° of Al cladding on the sides and on the sides and front of a 3″ × 3″ crystal. The calculations somewhat overestimate the reduction in ε° since here, as elsewhere, counts from scattered photons which would be part of the experimental photopeak are *not* included in ε° (except in section 5.2.1). The effect on the absolute detection efficiency $\varepsilon^\circ\ \varepsilon_{tot}$ is negligible when there is no front face and is given by the attenuation in the front face when there is a face (but see below).

Fig. 4 shows as a function of energy, the effects on various peak efficiencies and peak fractions of 3.2 mm (1/8″) of Al_2O_3 around a 3″ × 3″ NaI in a broad parallel beam of photons. The first thing to note is that the effect on the absolute photopeak efficiency is accurately predicted by calculating the number of interac-

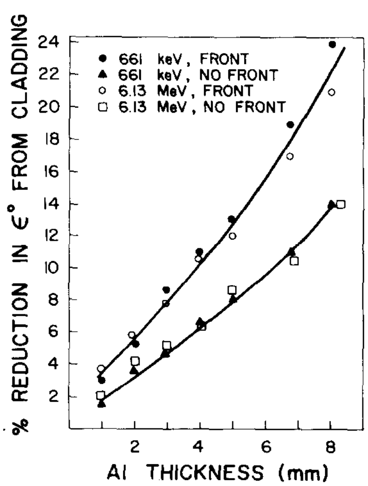

Fig. 3. The calculated percentage reduction in ε° for broad parallel beams of 661 keV and 6.13 MeV photons incident on a 3″×3″ NaI detector clad in varying thicknesses of Al. The solid lines are visual guides only. The upper points correspond to there being a complete Al case around the detector, including on the front face, the lower ones to the case without the front face.

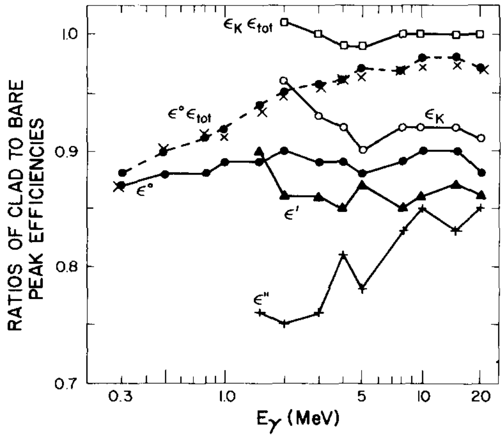

Fig. 4. Effects, as a function of photon energy, of 3.2 mm of Al_2O_3 around a 3″×3″ NaI detector in broad parallel beams of photons. The ratio of the clad to the bare values of absolute efficiencies and peak fractions are shown except for the crosses which show the fraction of incident photons *not* interacting in the front face. The reductions are overestimated since photons losing only a small amount of energy are considered lost from the peaks (see section 5.2.1). Note that the cladding has virtually *no* effect on the absolute detection efficiency for the top 1.5 MeV of the spectrum and that the effects on ε°, ε' and ε'' are considerably different (this would be important for Ge(Li) detector calculations).

tions in the front face. The second important feature is that the effects on ε°, ε' and ε'' differ considerably, the escape peaks being reduced by more than the photopeak. Further calculations have shown this is because 511 keV photons which would escape from a bare detector are sometimes reflected back into the detector, thus removing the count from the escape peak. The double escape peak is reduced more because only one of the two escaping 511's need be reflected to remove the count from the peak. This effect will not be important when using NaI detectors but could be significant with Ge(Li) detectors. A third feature is that the number of counts within 1.5 MeV of the photopeak ($\varepsilon_K\ \varepsilon_{tot}$) is virtually unchanged by the presence of the jacket, despite the fact that above 2 MeV, 2–5% of the photons interact in the front face of the jacket. This means that if the entire high energy portion of a spectrum is being used to determine photon intensity, attenuation by the front face should *not* be explicitly accounted for when calculated bare crystal efficiencies are used.

5.2.3. *The 511 keV peak*

Another effect of encapsulation is to produce a 511 keV peak in the spectrum from detection of an annihilation gamma-ray produced after pair production in the jacket. For a 3.2 mm layer of Al_2O_3 about a 3″ × 3″ NaI the 511 keV peak represents about 0.4–0.6% of the response to broad parallel beams of 3 to 20 MeV gamma-rays. However the effect is much more dramatic if even a thin lead shield is placed around the detector in order to reduce the X-ray count rate.

This is shown in fig. 5, where the 511 keV peak is actually the tallest peak in the spectrum for a 6.13 MeV beam incident on a 5″ × 4″ NaI detector covered by a 3 mm lead shield. The 511 peak contains 4% of the counts in the spectrum whereas the photopeak has 15%. The lead increases the counts below 1 MeV from 3% to 16% of the spectrum.

Although encapsulation qualitatively explains the existence of the 511 keV peak, experimentally there are many more 511 counts than calculated. The effects of the room are obviously important.

5.2.4. *The backscatter peak*

A prominent feature in many experimental NaI spectra is a "backscatter" peak at about 200 keV. The present calculations do produce signs of such a peak but it is usually much smaller and broader than the corresponding experimental data. For example, a 3.2 mm layer of Al_2O_3 around a 3″ × 3″ NaI detector in a broad parallel beam of photons with energies between 500 and 3000 keV produces a "peak/lump" with an area corresponding to only 2% of the spectrum. Even abnormally large amounts of material behind the detector do not significantly change this "peak" so it is not due to backscatter from the photomultiplier tube.

The program was modified to place the source be-

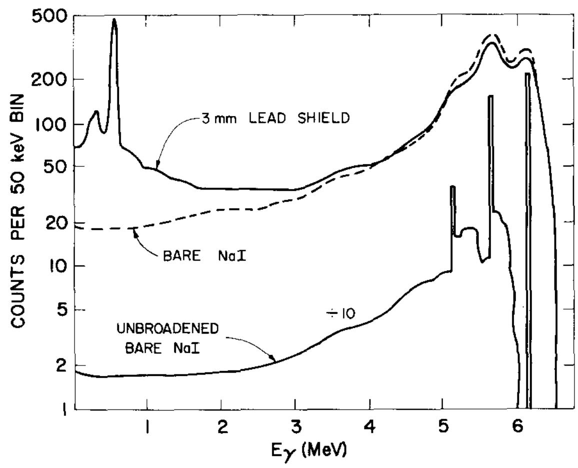

Fig. 5. Effects of a 3 mm lead shield around a 5″×4″ NaI detector irradiated by a 6.13 MeV gamma source at 100 cm. The 511 keV peak comes from pair production in the lead shield. The unbroadened bare NaI spectrum is shown reduced by a factor of 10. The large fraction of the high energy counts which are Compton events makes it difficult to experimentally measure peak efficiencies. The counts per bin shown are per 1.31×10^7 isotropic source photons into 4π.

tween the front face of the cladding and the detector. In this case a considerably sharper and hence more prominent peak was obtained because the face scattered photons at back angles into the detector. This is not a realistic situation but does indicate the backscatter peak is primarily a room effect and likely due to material on the far side of the source from the detector.

5.3. Comparison to experiments for NaI detectors

There have been a wide variety of NaI response function measurements reported (see Heath's review [29] for references). Detailed comparison between theory and experiment is often difficult because the experimental conditions are not completely specified (e.g. jacket thicknesses, sources of scattering, etc.). In many comparisons of calculations and experiment it has been found that the absolute photopeak efficiency is reasonably well reproduced whereas the calculated photofraction is too high. In what follows a few selected comparisons are presented to indicate the extent to which inclusion of the encapsulation improves the calculations.

Before making comparisons to experiment it is worth noting the unbroadened spectrum in fig. 5 which shows that roughly 50% of the counts in the high energy region of the spectrum are from Compton events. This Compton background makes it difficult to extract an accurate experimental measure of the "photopeak efficiency" as calculated by a Monte Carlo calculation since the background will inevitably be included in the measured photopeak.

Table 8 compares the present calculations to Jarczyk's experimental results [30] for the absolute photopeak efficiency of a 3″ × 3″ NaI detector in a broad parallel beam. The agreement is reasonable considering the experimental uncertainties. In all cases (except 10.8 MeV) the effect of including the cladding in the calculation is to improve the agreement.

Table 9 compares Waibel and Grosswendt's experimental results [9] to the calculations for the photopeak efficiency and for the high energy efficiency for a point source 10 cm from a 3″ × 3″ NaI. The agreement is generally very good. The clad results tend to move the calculated results closer to experiment although the cladding thickness included in the calculation is thicker than used in the experiment. As pointed out in section 5.1.1, the EGS results are closer to experiment than those calculated by Grosswendt and Waibel [8].

Table 10 compares Heath's experimental results [28] to the calculations of the photofraction ε° for a point source 10 cm from a thinly clad 3″ × 3″ NaI. The agreement is remarkably good for those "measurements" which do not include effects from the surroundings but this is tantamount to comparing photopeak efficiencies, not photofractions. In those cases in which the backscatter peak, etc., are included in the measurements, the calculated results are somewhat high since they do not completely explain these effects.

Table 8
Comparison of Jarczyk et al.'s [30] measured and the present calculated absolute photopeak efficiencies for broad parallel beams of photons incident on a 3″×3″ NaI detector.

E_γ (MeV)	Absolute photopeak efficiency		
	Expt	Calculated	
	Jarczyk [a]	Bare	Clad 3.2 mm Al_2O_3 [b]
0.661	0.44	0.493	0.448(5)
1.33	0.27	0.296(6)	0.276(6)
2.75	0.136	0.148(4)	0.141(4)
5.43	0.069	0.075(2)	0.073(2)
7.38	0.043	0.053(3)	0.051(3)
10.83	0.031	0.028(1)	0.027(1)

[a] Average of two values in fig. 7 of ref. 30. Uncertainties ≤8–12%.
[b] This is likely a "worst case" for the cladding since explicit information is not given in the original paper.

Fig. 6 presents a comparison between calculation and Heath's measurement for 662 keV photons incident on a 3″ × 3″ NaI behind a 1.18 g/cm² Be beta absorber. The calculated results have been broadened using the detector's measured resolution but otherwise there are no free parameters. The calculation accurately accounts for the "filling in" of the valley below the photopeak

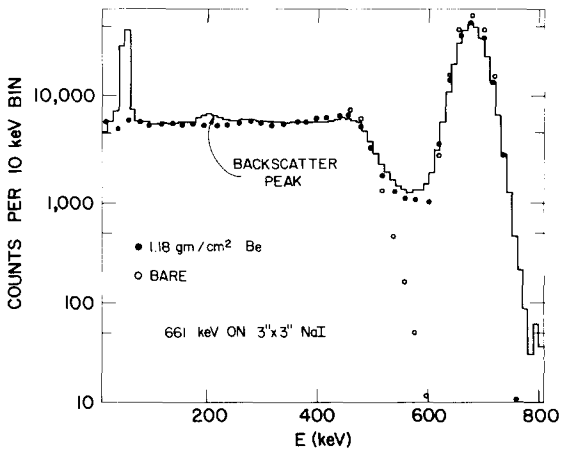

Fig. 6. Measured and calculated response of a 3″×3″ NaI detector with a 1.18 g/cm² beta absorber to 3.07×10⁷ 661 keV photons from an isotropic source 10 cm away. The open circles represent the calculations with no absorber. The inclusion of the absorber accounts for the filling in of the valley. The experimental spectrum is from Heath [28]. There are no free parameters in the calculation.

Table 9
Comparison of calculated EGS results to Waibel and Grosswendt's [9] measured values of $\varepsilon^{\circ}\,\varepsilon'_{tot}$, the intrinsic photopeak efficiency and $\varepsilon_K\,\varepsilon'_{tot}$, the high energy efficiency, for a point source 10 cm from a 3″×3″ NaI detector.

E_γ (MeV)	$\varepsilon^{\circ}\,\varepsilon'_{tot}$			$\varepsilon_K\,\varepsilon'_{tot}$		
	Expt [a)]	Calculated		Expt	Calculated	
		Bare	Clad [b)]		Bare	Clad [b)]
0.511	0.41	0.43	0.39			
0.835	0.27	0.29	0.27			
1.276	0.185	0.20	0.18			
2.00	0.12 [c)]	0.13	–			
2.75	0.093	0.096 (3)	0.089 (3)	0.36	0.33(1)	0.32(1)
4.00	0.065 [c)]	0.069 (2)	0.063 (1)	0.30 [c)]	0.29(1)	0.28(1)
6.00	0.042 [c)]	0.041 (1)	0.038 (1)	0.25 [c)]	0.26(1)	0.25(1)
8.00	0.029 [c)]	0.032 (2)	0.030 (2)	0.22 [c)]	0.23(1)	0.22(1)
12.00	0.020 [c)]	0.017 (1)	0.015 (1)	0.18 [c)]	0.17(1)	0.16(1)
15.00	–	0.0089(5)	0.0083(5)	0.16 [c)]	0.11(1)	0.11(1)

a) Experimental uncertainties ≤5%.
b) Cladding is 3.2 mm of Al up to 2.75 MeV and 3.2 mm of Al_2O_3 above.
c) From interpolation line given in ref. [9].

and for the attenuation of the photopeak by the Be absorber.

At NRCC a source of 6.13 MeV gamma-rays from the $^{19}F(p,\alpha\gamma)^{16}O$ reaction is available and the fluence of 6.13 MeV gamma-rays has been absolutely calibrated by counting the associated alpha particles [31]. Fig. 7 shows comparison between experiment and calculations for the 6.13 MeV photons incident on a 5″×4″ NaI detector. The calculated response is in good agreement with the experimental results for the high energy region. For the integrated counts above 4 MeV the calculations and experiment agree to well within the 2% uncertain-

Table 10
Comparison of Heath's measured [28] and EGS calculated photofractions, ε°, for isotropic sources 10 cm from a 3″×3″ NaI with a thin Al jacket.

E_γ (MeV)	Expt Heath [c)]	EGS	
		Bare	Clad [a)]
0.320	0.820	0.836(3)	0.826(3)
0.662	0.536	0.566(3)	0.559(2)
0.835	0.474	0.498(2)	0.492(2)
1.33	0.357 [b)]	0.366(5)	0.361(5)
1.78	0.290	0.319(2)	0.315(3)
2.75	0.225 [b)]	0.227(3)	0.224(2)
3.13	0.207 [b)]	0.209(4)	0.206(4)

a) 0.3 mm around sides plus 7.4 mm at back to simulate the photomultiplier. Recall that the uncertainty in the ratio of bare to clad is more accurately known than suggested by the absolute uncertainties.
b) Measurement consisted of measuring photopeak area from source of known strength and dividing by a calculated total efficiency, thus not "measuring" the effect of backscatter and 511 keV peaks.
c) It is assumed, but not absolutely clear, that no Be absorber was used in ref. 28. [Note added in proof: Heath points out that a Be absorber was used. Values without the Be were 0.825 and 0.484 at 320 and 835 keV, respectively.

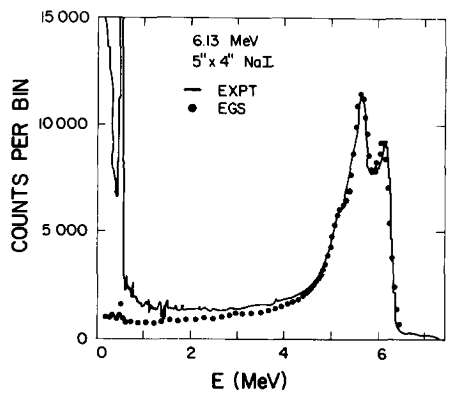

Fig. 7. An absolute comparison of the calculated and measured response of a 5″×4″ NaI detector in a known fluence of 6.13 MeV photons. After accounting for a 2% feed to higher states, the integrated counts above 4 MeV are reproduced within the 2% uncertainty of the measurement. The 3.2 mm cladding of Al_2O_3 around the detector does not account for the large peak at 511 keV. Room background has been subtracted.

Table 11
Variation as a function of distance in the counts above 4 MeV per 6.13 MeV photon incident on the face of a bare 5″×4″ NaI detector.

Source distance (cm)	$\varepsilon_{>4}\ \varepsilon'_{tot}$	Normalized to ∞
∞	0.585(4)	1.000
300	0.567(4)	0.969(10)
100	0.539(2)	0.921 (7)
35	0.471(4)	0.713 (7)

ties. However the qualitative agreement is poor for the low energy part of the spectrum.

5.3. Distance effects

It is well known that as well as solid angle effects, the efficiency of a detector changes with distance because of edge effects, or alternatively because the solid angle to an effective centre should be used. The size of this effect is larger than I expected and hence table 11 is included to emphasize the importance of using efficiencies calculated for the appropriate distance. The intrinsic efficiency for a 6.13 MeV source 100 cm from a 5″ × 4″ NaI is in fact 8% less than if the source were a broad parallel beam. The effect is 3% for a source even 3 m away.

6. Response functions for Ge(Li) detectors

The major thrust of this study was to study the response functions of NaI detectors but the versatility of the EGS system means the code JACKET can handle the case of Ge(Li) detectors equally well. Simple modifications were made to the energy scoring routine to allow for "inert" volumes in the detector where the photons and electrons are transported as usual but no energy depostion is included in the scoring since these regions are not sensitive. The effects of these inert volumes will be discussed below. In keeping with many previous calculations of Ge(Li) response functions, fig. 8 presents a comparison of the calculated double escape peak efficiencies for isotropic point sources 1.6 cm from Ewan and Tavendale's [32] small planar Ge(Li) detector which was 1.8 cm in diameter and 3.5 mm thick. The EGS calculations are in reasonable agreement with the experimental data, comparable to Wainio and Knoll's calculations at lower energy but considerably lower above 6 MeV [33], and somewhat higher than Grosswendt and Waibel's calculations [10] as was also the case with their calculations for NaI detectors [8]. For the sake of comparison, the EGS calculations shown in fig. 8 were done for a bare detector with no inert re-

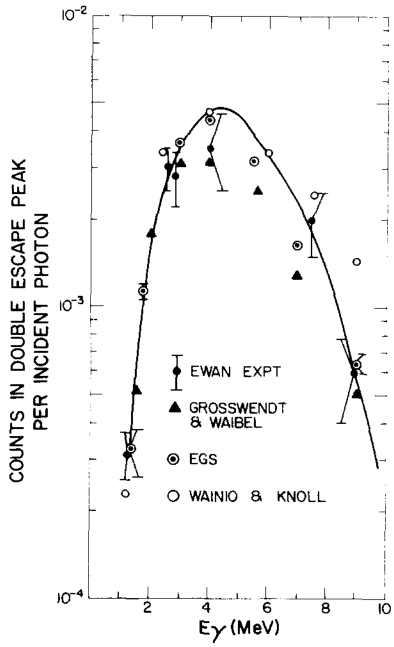

Fig. 8. Double escape peak efficiency for an isotropic source 1.6 cm from Ewan and Tavendale's [32] Ge(Li) detector which was 1.8 cm in diameter and 0.35 cm thick.

gions. More realistic calculations can be done which take into account the 3 mm lucite front plate holding the detector in place, the 0.2 mm n^+ inert layer on the front of the detector, and the 6.3 mm inert layer of Ge behind the 3.5 mm active detector volume. The effect of this increased sophistication is to reduce the absolute double escape peak efficiency by $2 \pm 5\%$ at 5.5 MeV and $13 \pm 5\%$ at 3.0 MeV and to increase the calculation time by 20–30%. Calculations of the photopeak efficiency and photofraction of Ewan's counter for photons between 400 keV and 1400 keV are in agreement with the calculations of Wainio and Knoll. The calculated photopeak efficiencies agree with the measured efficiencies to within 10% but the calculated photofractions are substantially high (up to 70%). Even the more sophisticated calculations with a lucite holder and inert layers reduce the photofraction by only 10%.

Fig. 9 presents calculated and experimental results for the 26 cm³ true coaxial Ge(Li) detector described by Waibel and Grosswendt [9]. Two features stand out. The results calculated by EGS are typically 20% higher than the measured values and the calculated EGS results are higher than those calculated by Grosswendt and Waibel. A similar discrepancy in calculated values for NaI detectors was noted in section 5.1 where it was argued that the problem was with Grosswendt and Waibel's calculation. In the NaI case, the experimental results confirmed the EGS calculations whereas for Ge(Li) detectors they appear to support Grosswendt

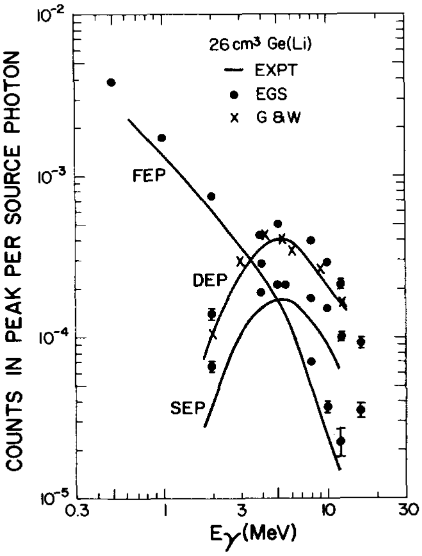

Fig. 9. Calculated and measured peak efficiencies for isotropic sources 4.80 cm from a 26 cm^3 Ge(Li) detector. The measured efficiencies and calculated double escape peak efficiencies shown with crosses are from Grosswendt and Waibel [9,10]. Neither set of calculations included the effect of dead layers although these are important.

and Waibel's calculations. This agreement is more apparent than real since neither set of Ge(Li) calculations took into account the inert layer on the detector's cylindrical surface or the detector's jacket.

The effect of the jacket on the double escape peak efficiency is hard to calculate without doing a full calculation since the reduction is greater than expected due simply to attenuation in the jacket (see section 5.2). For the 26 cm^3 detector discussed above, if we assume a 2 mm Al jacket around the crystal plus 1 cm at the rear to represent the cold finger, then 1.3% to 2.4% of photons with energies in the range 2–10 MeV interact in the front face but there is a 4.3% to 7.7% reduction in the absolute double escape peak efficiency.

As well as the effect of the jacket, there is the effect of the inert dead layer on the detector's outer cylindrical surface. The layer is an intrinsic part of the detector's construction. Unfortunately the depth of this layer may change with time and its boundaries are both diffuse and hard to specify. Fig. 10 shows the effects of including up to a 2 mm inert layer about the 26 cm^3 detector. A 2 mm layer reduces the active detector volume by 21%. The detector's total efficiency is not reduced this much because events which scatter between the active and inert layers are still registered. However, the effects on the peak efficiencies are clearly of the same order, if not greater than the volume reduction. This strong dependency on the thickness of the inert layer makes it virtually impossible to do a reliable calculation of the

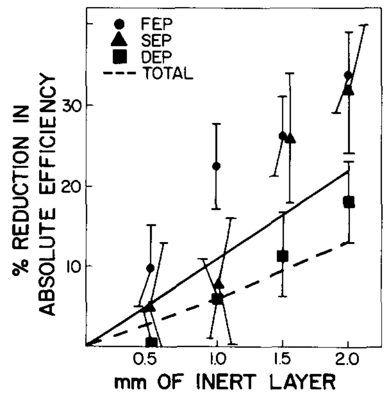

Fig. 10. Effects of an inert layer on the calculated efficiencies of a bare 26 cm^3 coaxial Ge(Li) detector for 5 MeV photons. The solid line gives the volume reduction of the active detector as the inert layer increases. The sensitivity of this parameter makes accurate calculations of Ge(Li) detector absolute efficiencies very difficult.

absolute efficiency of a Ge(Li) detector unless the counter's inert layers can be accurately specified (see below for a discusion of relative efficiency curves).

In conclusion, the 20% discrepancy between the calculated EGS results and the experimental results of Grosswendt and Waibel do not seem significant in view of the large effects expected if the detector jacket and inert layers were taken into account.

Recently, Raudorf et al. [34] of Ortec have published a detailed report on the characteristics of a 35% intrinsic germanium detector. They report its efficiency for a source 25.5 cm from the crystal face is 4.2×10^{-4} counts in the full energy peak per 1.33 MeV gamma ray from the source. Characterising the detector as 5.70 cm in diameter, 6.40 cm long, with an inert surface layer of 0.05 cm, an inert core of 0.8 cm, and having an Al jacket around the detector, 0.5 mm thick in front, 1 mm thick on the sides and 6 mm thick on the back, EGS calculates an efficiency of $4.69 \times 10^{-4} \pm 1.6\%$ or 12% higher than measured.

Fig. 11 presents an experimental relative efficiency curve for a 74 cm^3, 5 sided, cylindrical Ge(Li) detector in use at NRCC [35] (4.9 cm diameter, 4.1 cm long, 1.75 cm drift depth, 0.8 cm diameter inert core at the back and a 2 mm Pb filter on the front face). Also shown are two calculated relative efficiency curves (normalized at 1.33 MeV), one calculated with no inert layers and the second with a 1 mm inert layer on the outer surface. Although the inert layer has about a 15% effect on the absolute calculated efficiencies, the effect on the relative efficiencies is much less, especially for the photopeak. The agreement between calculation and experiment is quite acceptable, especially the photopeak efficiency for which agreement to within 10% is achieved for an

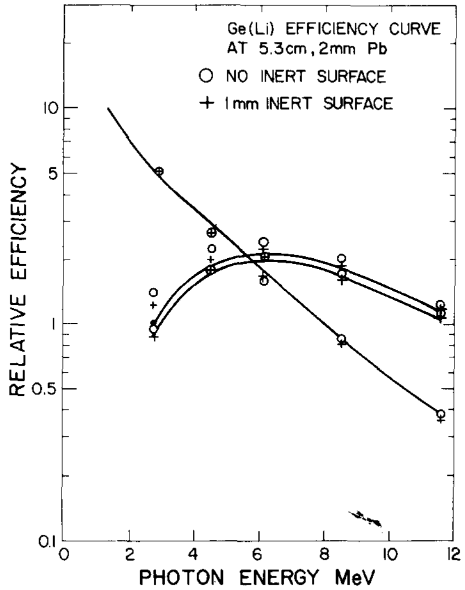

Fig. 11. Calculated and measured relative efficiency curves for the 74 cm^3 coaxial Ge(Li) detector specified in section 6. All data are normalized to the efficiency at 1.33 MeV and refer to isotropic point sources 5.3 cm away from the detector which was shielded by a 2 mm lead face plate. The open circles refer to calculations with no inert surface layer and the × to those with a 1 mm inert surface layer. Although there was a 20% change in the absolute efficiencies in these two cases, the effect on the relative efficiency curves was much smaller.

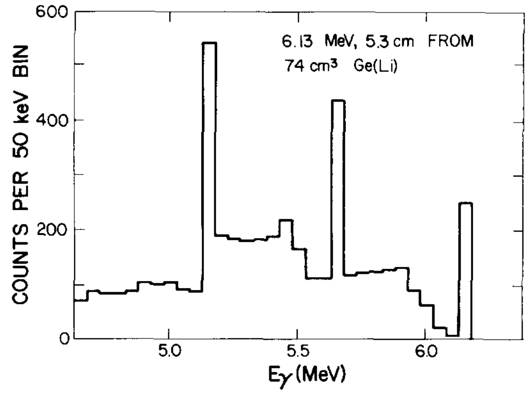

Fig. 12. Calculated high energy response of the 74 cm^3 coaxial Ge(Li) detector specified in section 6 to an isotropic source of 6.13 MeV photons at 5.3 cm distance. The step function in the background around the double escape peak is clearly visible.

efficiency varying by a factor of 26. The situation for the calculated absolute efficiency is much less satisfactory, the EGS results being 25% (with a 1 mm inert layer) or 50% (no inert layer) larger than the measured value. This probably reflects problems with charge collection and/or our ignorance of the depth of the inert layers and/or the true shape of the sensitive volume (see e.g. refs. 5, 36).

Fig. 12 presents the upper portion of the calculated response for 6.13 MeV gamma-rays on the 74 cm^3 detector discussed above. The spectrum shows clearly the step observed about the double escape peaks. These correspond to Compton scattered 511 keV photons escaping, leaving less than 511 keV in the detector, and thus appearing on one side of the peak only.

In summary, EGS can be used to calculate the response functions of Ge and Ge(Li) detectors for photons above 300 keV. The calculated absolute efficiencies tend to be too large and are not expected to reproduce the experimental data as accurately as in the case of NaI detectors because of uncertainties in the specification of the sensitive volume of the Ge and Ge(Li) detectors. However, there are indications that the calculated relative efficiency curves are reasonably accurate since they are not as sensitive to details of the detector geometry.

7. Other calculations

In the following sections, a variety of calculations done with JACKET are presented in order to indicate the code's versatility.

7.1. Electron detectors

JACKET can be used to calculate response functions for electron detectors by changing the charge of the incident particle from 0 to −1. Comparisons have been made with CYLTRAN calculated response functions for electrons with energies between 500 keV and 8 MeV incident on Si and Ge detectors 1 to 20 mm thick and 10 to 50 mm in diameter. In some cases there was a factor of 3 disagreement until the maximum step size used in EGS was substantially reduced. After the reduction the agreement was excellent, even at the lower energies where the multiple scattering formalism used in EGS is expected to break down (electron cut-offs of 10 to 30 keV were used). Further work is being done to optimize the use of EGS in this region since the currently used step size limit causes the computing time to increase by up to a factor of 10.

Comparisons have also been made to the results of Berger and Seltzer [4] for electrons on a small Si detector. Agreement is acceptable if a large detector radius is used for the EGS calculations but Berger and Seltzer's calculation using an infinite slab geometry does not apply to their experimental detectors for energies above 1 MeV. For example, for a 5 MeV electron beam incident on a 10 mm thick Si detector, $\varepsilon^\circ = 0.23(1)$ for a 1 cm diameter detector whereas $\varepsilon^\circ = 0.52(1)$ for an infinite diameter.

7.2. Bismuth germanate detectors

Bismuth germanate ($Bi_4Ge_3O_{12}$) is gaining acceptance as a photon spectrometer in situations where small size and high efficiency are more important than good resolution. Fig. 13 presents a comparison of the peak efficiencies for 3" × 3" bismuth germanate and NaI detectors for photon source 10 cm away. At 1 MeV the bismuth germanate is 2.4 times as efficient at detecting the photopeak as the NaI detector is. Another way of looking at it is that a $3'' \times \frac{1}{2}''$ bismuth germanate detector's photopeak efficiency for a 500 keV source 10 cm away is still 32% greater than that for a 3" × 3" NaI.

7.3. 70 MeV positrons into TINA

TINA is an 18" × 20" NaI detector used at TRIUMF to detect high energy positrons. The positron beam must pass through a series of veto and accept counters and the container before entering the NaI detector. This material has been simulated with JACKET as a 1.6 cm layer of polystyrene on the face of the detector. Fig. 14 shows the calculated response function for a pencil beam of 70 MeV positrons before and after broadening to fit the observed resolution. The comparison to experiment [37] is only valid concerning the tail on the lineshape since the area, resolution and centroid position were all adjusted. As can be seen, the distinct full energy and single escape peaks in the raw calculation are completely washed out by the detector's resolution function. The importance of doing a coupled calculation with the veto/accept counters and the NaI is illustrated by the following. Based on Berger and Seltzer's energy loss tables [22] a pencil beam of 70 MeV positrons loses ~2.1 MeV via bremsstrahlung losses and 3.4 MeV via collisional losses in a 1.6 cm polystyrene slab. However there is only a (3.0 ± 0.1) MeV shift in the centroid of the calculated response functions with and without the polystyrene in place, indicating that 45% of the energy lost by the positrons in the polystryene was detected in the crystal. This fact points out the need for the coupled calculations. Work on TINA's response functions is still in progress, investigating the effects of the choice of energy cut-offs, Landau effects, etc.

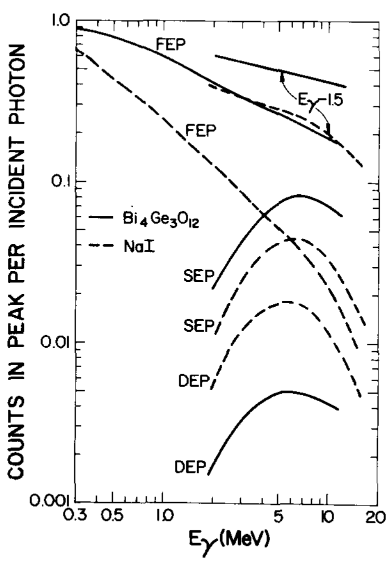

Fig. 13. A comparison of the calculated efficiencies of bare 3"×3" bismuth germinate and NaI detectors for sources 10 cm away.

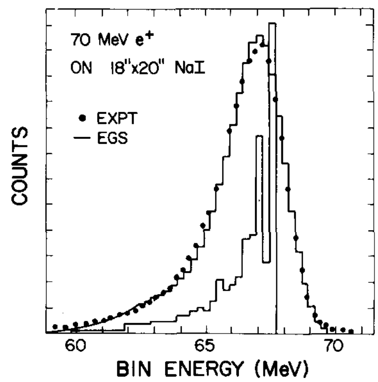

Fig. 14. Calculated and measured response of TINA to 70 MeV positrons. TINA is an 18"×20" NaI detector with various veto/accept counters on its front face which have been simulated by a 1.6 cm layer of polystyrene. Only the lineshape comparison is of interest since the resolution, area and energy calibration have been adjusted. [ECUT, PCUT]=[1.5 MeV, 100 keV].

7.4. Finite solid angle correction factors

When nuclear detectors are used to study the angular distributions of gamma decays, correction factors must be applied to take into account the detector's finite size. These factors are defined as

$$Q_k = I_k / I_0,$$

with

$$I_k = \int_\Omega \eta(\theta) P_k(\cos\theta)\, \mathrm{d}\Omega,$$

where $\eta(\theta)$ is the detection probability for a photon leaving the source at an angle θ with respect to the detector's axis and $P_k(\cos\theta)$ is the kth order Legendre polynomial (only Q_2 and Q_4 are important in practice). In general Q_k coefficients for Ge(Li)'s have been calculated using an analytical $\eta(\theta)$ based on the probability for any interaction (e.g. ref. 38) and these factors were then applied to any or all three of the observed peaks.

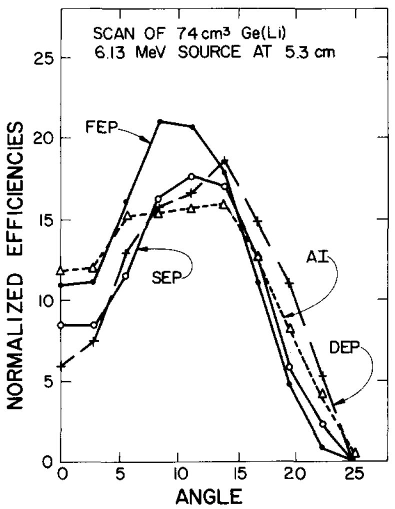

Fig. 15. Normalized efficiencies for various peaks as a function of scan angle for a pencil beam starting 5.3 cm from the 74 cm^3 Ge(Li) detector specified in section 6. The curve marked AI is for any interaction in the detector.

However, in principle one would expect the efficiencies as a function of angle to be different for each peak.

Fig. 15 confirms this fact by plotting $\eta(\theta)/I_0$ for each of the three peaks and for "any interaction" [for a source 5.3 cm from the 74 cm^3 Ge(Li) detector described in section 6]. As expected, the double escape peak is the "most efficient" towards the surface where the probability of two photon escape is highest. Since I_k is weighted by a $\sin\theta$ term, the major effects come from the values at the larger angles. From the figure one would therefore expect $Q_k(\mathrm{DEP}) \leqslant Q_k(\mathrm{AI}) \leqslant Q_k(\mathrm{FEP}) \leqslant 1$, where $Q_k = 1$ implies no correction. Indeed the attenuation coefficients calculated using these scan values are: $Q_2(\mathrm{DEP}) = 0.898$, $Q_2(\mathrm{AI}) = 0.906$, $Q_2(\mathrm{FEP}) = 0.924$ and $Q_4(\mathrm{DEP}) = 0.687$, $Q_4(\mathrm{AI}) = 0.710$ and $Q_4(\mathrm{FEP}) = 0.762$. These results qualitatively confirm the findings of Borresen and Ingebretsen [6] who have studied this question in detail although EGS calculates considerably different efficiencies from those they have calculated.

8. Conclusions

The code JACKET and the simulation package EGS have been used to calculate response functions for a wide variety of nuclear detection systems. Detailed comparisons with a variety of codes calculating NaI response functions verifies the code's accuracy. There were however a few minor, but persistent discrepancies with the calculated peak efficiencies at high energies ($\geqslant$ 10 MeV) compared to ETRAN.

The results for Ge(Li) response functions were also satisfactory but less easily bench-marked against experiment due to uncertainties about inert volumes.

The calculations for Si and Ge electron detectors were less satisfactory until step size modifications were made and further work is being undertaken to optimize the use of EGS in this region.

One of the major advances of this study has been to study the effects of the detector's jacket on the response function. JACKET quantitatively explains the effects of Be beta absorbers on the response functions of NaI detectors and has qualitatively explained the existence of 511 keV peaks in the response function. On the other hand, this study shows that the detector's encapsulation and PMT do not make a large contribution to the backscatter peak.

The EGS system and the code JACKET are quite complex and hence I am reluctant to distribute is except to current users of EGS. However, it is simple to set up and run and an efort will be made to run specific cases for those making reasonable requests.

I would like to thank J. Sankey of NRCC for considerable programming help to get this project going. I would also like to thank Drs. W.R. Nelson, S.M. Seltzer and J.A. Halblieb Sr for long phone conversations about EGS, ETRAN and CYLTRAN respectively, and Drs. W.R. Dixon and L. van der Zwan for discussions about nuclear detectors and Dr. B. Grosswendt for information on his work. The codes EGS, ETRAN, MORN and CYLTRAN were all obtained from the Radiation Shielding Information Center at ORNL.

Appendix

Effects of energy cut-offs on running time

ECUT and PCUT are the energies below which all electrons and photons are assumed to deposit their energy locally (note electron energies include the rest mass). AE and AP are the cut-off energies used in PEGS to divide between continuous slowing down processes (knock-on electrons with energy $\leqslant$ AE, bremsstrahlung production of photons with energy $\leqslant$ AP) and discrete events (either scattering or photon production above the cut-off).

The code is most efficient if ECUT = AE and PCUT = AP since, for example, ECUT $\geqslant$ AE causes discrete events to be sampled and immediately discarded if the resulting electron energy is $\leqslant$ ECUT. Table 12 demonstrates this effect. However, in some cases it may be useful to use different values of ECUT and AE in order to more accurately simulate the statistical nature of energy loss.

Tracking photon histories is very fast but tracking

Table 12
Effects of changing the PEGS energy cut-offs AE and AP for a given pair of user energy cut-offs ECUT and PCUT. Times given are CPU times on a VAX computer for 20,000 6.13 MeV photons incident on a bare 5″×4″ NaI detector in a broad parallel beam. ECUT=700 keV (total energy) and PCUT=100 keV.

AE (keV)	AP (keV)	CPU time (s)	ε°
521	10	3129	0.202(3)
544	33	2337	0.202(5)
700	100	2091	0.199(2)

photons below 100 keV never appeared to make any difference in the computed value of ε°. Table 13 shows that PCUT = 300 keV saves some time but also has an effect on ε°. In most cases PCUT = 100 keV has been used but one consequence is that when there is no jacket in the calculation, there are no counts between E_0 and $E_0 - 100$ keV (assuming ECUT $\geq$ 100 keV) since there is no mechanism for $\leq$ 100 keV to escape from the detector.

The major determinant of running times is ECUT as shown in table 14. The major cost is in simulating the multiple scattering at low energies but the major effect is due to the creation of bremsstrahlung which escapes from the detector. In most calculations reported here, values of ECUT = AE = 0.7 MeV and PCUT = AP = 0.1 MeV have been used. At higher energies somewhat higher values of ECUT were sometimes used following the suggestion of Berger and Seltzer that ECUT = 0.511 + 0.04 × E_γ [2].

Table 13
Effect of changing PCUT, holding all other parameters fixed. The same test case as table 12 is used. ECUT=2511 keV, AE=521 keV, AP=10 keV.

PCUT (keV)	VAX CPU time (s)	ε°
10	763	0.223(3)
100	759	0.228(4)
300	713	0.261(4)

Table 14
Effects of ECUT on running time for test cases defined in table 12. AE=521 keV, PCUT=AP=10 keV.

ECUT (MeV)	VAX CPU time (s)	ε°	$\varepsilon_{>5\text{ MeV}}$
0.521	24860	0.202(12)	0.666
0.611	3564	0.198 (5)	0.661
0.700	3061	0.206 (3)	0.666
1.011	1838	0.207 (5)	0.675
1.511	1256	0.217 (5)	0.679
2.511	763	0.223 (3)	0.706
4.511 [a]	316	0.262 (3)	0.776
6.511	170	0.286 (3)	0.810

[a] PCUT=100 keV.

References

[1] M. Belluscio, R. de Leo, A. Pantaleo and A. Vox, Nucl. Instr. and Meth. 118 (1974) 553.
[2] M.J. Berger and S.M. Seltzer, Nucl. Inst. and Meth. 104 (1972) 317.
[3] M.J. Berger, in Methods in computational physics, vol. 1 (Academic Press, New York, 1963) pp. 135–213.
[4] M.J. Berger, S.M. Seltzer, S.E. Chappell, J.C. Humphreys and J.W. Motz, Nucl. Instr. and Meth. 69 (1969) 181.
[5] C. Birattari and A. Salomone, Nucl. Instr. and Meth. 174 (1980) 391.
[6] C.N. Borresen, F. Ingebretsen and S. Backe, Nucl. Instr. and Meth. 154 (1978) 535.
[7] M. Giannini, P.R. Oliva and M.C. Ramorino, Nucl. Instr. and Meth 81 (1970) 104.
[8] B. Grosswendt and E. Waibel, Nucl. Instr. and Meth. 133 (1976) 25.
[9] E. Waibel and B. Grosswendt, Nucl. Instr. and Meth. 131 (1975) 133.
[10] B. Grosswendt and E. Waibel, Nucl. Instr. and Meth. 131 (1975) 143.
[11] E. Nardi, Nucl. Instr. and Meth. 83 (1970) 331.
[12] J.J. Steyn, R. Huang and D.W. Harris, Nucl. Instr. and Meth. 107 (1973) 465.
[13] C.D. Zerby and H.S. Moran, Nucl. Instr. and Meth. 14 (1961) 115.
[14] R.L. Ford and W.R. Nelson, The EGS code system, Stanford Linear Accelerator Center Report No. 210, Stanford, CA (June 1978) and W.R. Nelson in W.R. Nelson and T.M. Jenkins (eds.), Computer techniques in radiation transport and dosimetry (Plenum Press, New York, 1980).
[15] J.A. Halbleib Sr. and W.H. Vandevender, Nucl. Sci. Eng. 61 (1976) 288.
[16] E. Storm and H.I. Israel, At. Data Nucl. Data Tables 7 (1970) 565.
[17] H.W. Koch and J.W. Motz, Rev. Mod. Phys. 31 (1959) 920.
[18] W. Heitler, The quantum theory of radiation (Clarendon Press, Oxford, 1954).
[19] H.A. Bethe, Phys. Rev. 89 (1953) 1256.
[20] S. Goudsmit and J.L. Saunderson, Phys. Rev. 57 (1940) 24 and Phys. Rev. 58 (1940) 36.
[21] H. Messel and D.F. Crawford, Electron–Photon shower distribution function (Pergammon Press, Oxford, 1970).
[22] M.J. Berger and S.M. Seltzer, NASA SP-3012 (1964).
[23] T.W. Armstrong and R.G. Alsmiller Jr, Nucl. Instr. and Meth. 82 (1970) 289.
[24] R.M. Sternheimer and R.F. Peierls, Phys. Rev. B3 (1971) 3681.

[25] M.D. MacLaren and G. Marsaglia, J. Assoc. Comp. Mach. 12 (1965) 83.
[26] G. Marsaglia, Random numbers fall mainly in the planes, Proc. NAS 61 (1968) 25.
[27] A.J. Cook and L.J. Shustek, SLAC Computation Research Group report CGTM no. 165 (1975).
[28] R.L. Heath, Scintillation spectrometry, gamma-ray spectrum catalogue, USAEC Report IDO-16880-1 (1964).
[29] R.L. Heath, R. Hofstadter and E.B. Hughes, Nucl. Instr. and Meth. 162 (1979) 431.
[30] L. Jarczyk, H. Knoepfel, J. Lang, R. Müller and W. Wölfli, Nucl. Instr. and Meth. 17 (1962) 310.
[31] D.W.O. Rogers, in preparation.
[32] G.T. Ewan and A.J. Tavendale, Can. J. Phys. 42 (1964) 2286.
[33] K.M. Wainio and G.F. Knoll, Nucl. Instr. and Meth. 44 (1966) 213.
[34] T.W. Raudorf, T.J. Paulus and R.M. Trammell, Nucl. Instr. and Meth. 176 (1980) 595.
[35] W.R. Dixon and R.S. Storey, private communication.
[36] I.S. Sherman and M.G. Strauss, Nucl. Instr. and Meth. 103 (1972) 113.
[37] M. Dixit, private communication.
[38] D.C. Camp and A.L. Van Lehn, Nucl. Instr. and Meth. 76 (1969) 192.